

Diffraction Imaging After Diffraction Separation in Data Domain

M. Protasov(✉)

Institute of Petroleum Geology and Geophysics, Novosibirsk 630090, Russia
protasovmi@ipgg.sbras.ru

Abstract. Diffracted/scattered waves are used to construct diffraction images and further seismic interpretation. There are various algorithms for their extraction, which can be divided into three classes regarding the data processing steps: data do-main procedures, migration-based methods, and image processing. The paper presents the algorithm for the data domain diffraction separation. Also, it provides an investigation of the influence of the diffraction separation in the data domain, focusing on the migration procedure based on the construction of selective images. Numerical experiments are performed using synthetic data obtained for a realistic model with fractures from the field in Eastern Siberia.

Keywords: Seismic data · Diffraction imaging · Diffraction separation

1 Introduction

Currently, in the practice of seismic research, diffraction images or images in scattered waves, as well as methods for their construction, are of increasing interest. This is primarily because of the need to search and develop fractured carbonate reservoirs [1]. According to various estimates, these reservoirs contain from 35 to 48% of the world's oil reserves and from 23 to 28% of the world's gas. The scattered component of the seismic wave field carries significant information about small-scale geological objects, in particular, fracture zones. Its processing makes it possible to localize such geologically interesting objects as zones of increased fracturing, faults and surrounding crushing zones, cavernous-fractured zones [2, 3].

Diffracted/scattered waves are used as additional information for the seismic interpretation. There are various algorithms for their extraction from the seismic data, which can be divided into three classes concerning the data processing workflow: in the data domain, during the migration and image processing. One of the first is the algorithm of diffraction moveout correction and stacking [4]. The paper by Fomel, Landa, and Taner introduces the so-called plane wave destructor for separating specular reflections and scattering/diffraction in the data space [5]. In this method, they get classical images but for the scattered/diffracted component of the wavefield. Moser and Howard develop the approach of diffraction imaging in the depth domain in the context of the pre-stack migration [6]. They use the two-stage implementation of the regular migration: employment of specular reflection on the first and their suppression and weakening on the

© The Author(s), under exclusive license to Springer Nature Switzerland AG 2022
O. Gervasi et al. (Eds.): ICCSA 2022 Workshops, LNCS 13382, pp. 560–571, 2022.
https://doi.org/10.1007/978-3-031-10592-0_40

second. Analysis of seismograms in the structural angles coordinate system reveals a significant difference in the reflected and diffracted waves in these coordinates. On this basis, efficient algorithms for separating reflection and diffraction/scattering are proposed and implemented [7, 8]. In this angle domain, for many cases, the reflection is convex, whereas the diffraction corresponds to a straight line. Therefore, the effective separation procedure here is filtering in the Radon transform domain [9, 10]. Decker, Merzlikin, and Fomel further develop seismic diffraction imaging utilizing the principle of flatness of diffraction events in slope gather together with the plane wave destructor [11]. Zhang and co-authors propose a wave-equation diffraction imaging procedure based on a decomposition of the wavefields into left- and right-downgoing propagating waves [12]. The proposed method adds reasonable additional computational cost over wave-equation reflection migration and therefore provides practical wave-equation-based diffraction imaging. Wang, Liu, and Chen present one more way to separate and imagine seismic diffractions based on a localized rank-reduction method using a local plane-wave assumption [13]. The proposed method shows advantages over the plane wave destructor and general rank reduction method.

Algorithms that use diffracted/scattered waves during migration are based on suppressing the energy of reflected waves. Still, they suppress some of the energy of the diffracted/scattered waves. Image processing algorithms have the same disadvantage. Diffracted/scattered waves can be extracted when working directly in the seismic data domain not ideally, but most of their energy remains [14]. This paper proposes the new workflow for the seismic data processing of the diffracted/scattered waves, where diffraction separation in the data domain is used before application of diffraction imaging procedure. The algorithm for diffraction separation is proposed, which is based on the different kinematic behavior of the reflected and scattered waves in the common offset domain. The influence of the diffraction separation in the data domain is investigated on the results of the diffraction imaging procedure based on the construction of selective images [15]. Numerical experiments are performed using synthetic data got for a realistic fractured model of the field in Eastern Siberia.

2 Diffracted Wave Estimation

The seismic data are supposed to contain reflected waves and diffracted/scattered waves. They are considered in the mid-point offset domain:

$$d(t, x_m, h) = ref(t, x_m, h) + dif(t, x_m, h), \tag{1}$$

where d is the seismic data, ref are reflected waves, dif are diffracted/scattered waves, (t, x_m, h) are time, mid-point, and offset coordinates, respectively. The algorithm for separating diffracted/scattered waves dif from the seismic data d is based on the essentially different kinematic behaviour of reflected waves and diffracted/scattered waves in the common offset domain. Hodograph of the reflected wave in that domain $t_{ref}(x_m)$ «follows» the corresponding reflected interfaces, and usually, they provide locally plane events, however the hodograph of diffracted/scattered wave $t_{ref}(x_m)$ has behavior where second-order derivatives have significant influence:

$$t_{ref}(x_m) \approx t_0 + a \cdot x_m; \tag{2}$$

$$t_{dif}(x_m) \approx t_0 + a \cdot x_m + b \cdot x_m^2. \tag{3}$$

One can observe such behavior on a simple model example with two horizontal layers and four point scatters (Fig. 1). The reflection wave represents flat event while diffractions have significant curvature. Such a different behavior provides a wide range of algorithms [14].

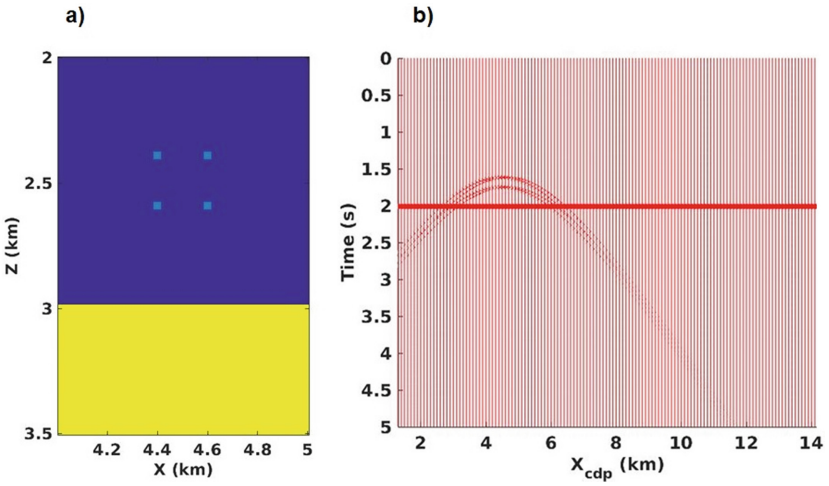

Fig. 1. a) Simple model with flat interfaces and point scatterers. b) The corresponding seismic data in the common offset domain.

The proposed here algorithm is a combination of two most effective techniques. The first part of the procedure comprises enhancing reflected waves [16] and suppressing all the other events, including diffractions followed by reflections subtraction from the initial data (it is like one algorithm from [14]). At this stage, the enhancement procedure uses kinematic of the reflected events (2) at small apertures. At the second stage, algorithm provides enhancement of the diffracted/scattered waves and suppression of the redundant reflected events. Here, the enhancement technique uses an estimation of the kinematic of the diffracted/scattered waves and their usage at rather big apertures. The last part of the procedure is like the so-called multi-focusing technique oriented on diffractions [17]. Note, for the ideal data, the first part of procedure can provide satisfactory results when the reflections are rather clear and there is no big amplitude difference in reflections and diffractions. But, for realistic cases and real data, these are rather rare circumstances, therefore second part of the procedure provides improvement of the diffractions that were extracted at the first stage.

2.1 Ideal Diffracted Wave Identification

To exclude the errors and limits of the diffraction separation algorithm, ideal extraction of diffracted waves only is provided for simple and realistic synthetic models. For simple

synthetic model, such extraction is straightforward because an analytic solution can provide waves separately. For the realistic case, two synthetic models are created (Fig. 2a, 2b). Both models contain the objects of diffraction are located: one layer with fractures. The second model contains additional fracture layer that provides diffractions while first original model does not have them. In these models, synthetic data are calculated using the finite difference method (Fig. 2d, 2e). To get diffracted waves only that produced by the inhomogeneities corresponding to this bottom fractured layer of the second model (Fig. 2c), one should take the difference of the wave fields (Fig. 2d). This result provides the ideal separation of diffracted/scattered waves produced by the bottom fractured layer of the second model.

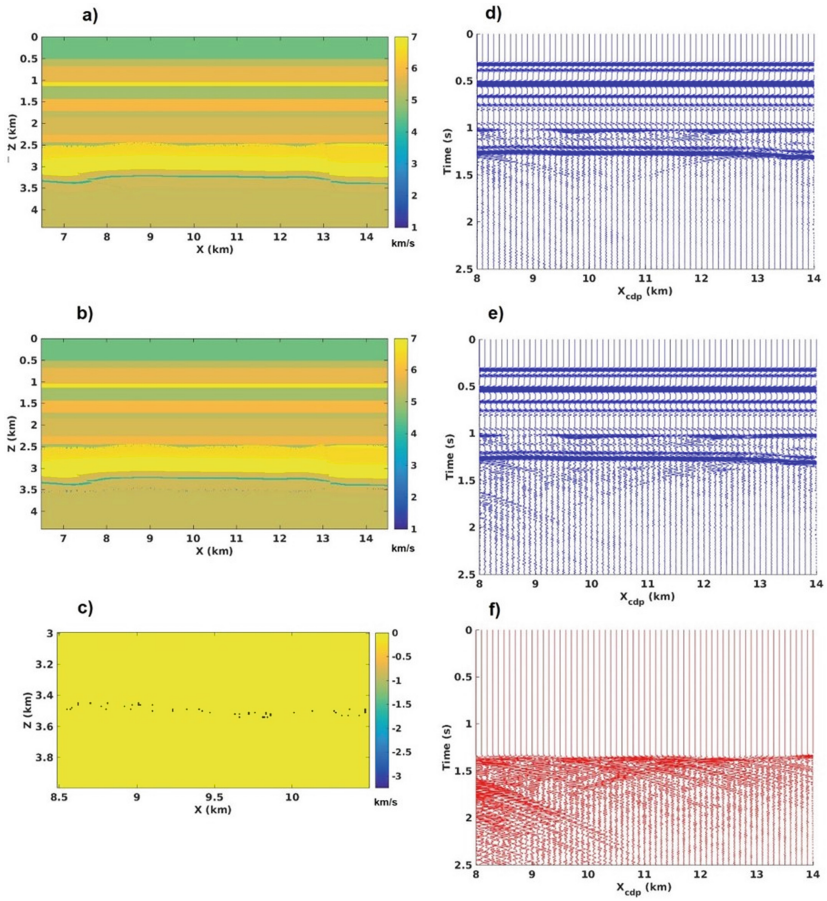

Fig. 2. a) Initial realistic model derived from seismic data. b) Realistic model with cracked layer. c) Difference of models in the region of the layer with cracks. d) Zero offset gather for the original model. e). Zero offset gather for a model with a fractured layer. f) Difference between seismograms d) and e).

2.2 Diffracted Wave Separation vs Ideal Identification

Then the described above algorithm for diffraction separation is applied to the data computed in a simple model and to the data generated in a realistic model. Results of diffraction separation for the data in the simple model show reflections are sup-pressed completely (Fig. 3b). Although the diffractions in this case do not coincide with the ideal result, the main kinematic and dynamic properties of the diffracted waves stay the same (Fig. 3).

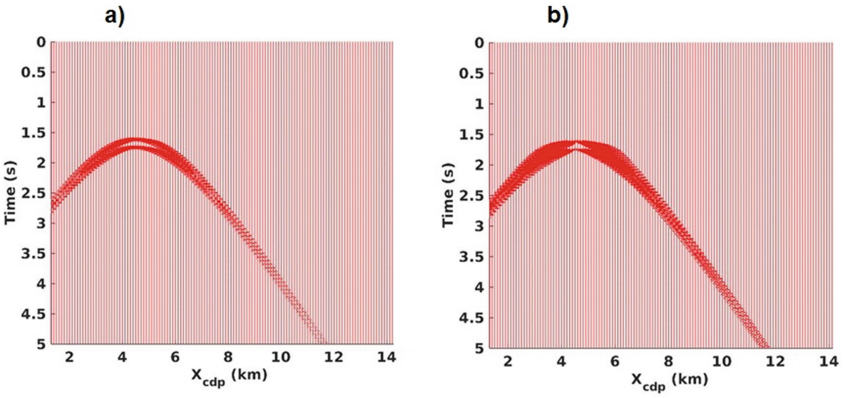

Fig. 3. Simple data: a) the ideal separation; b) results of the data domain diffraction separation.

Diffraction separation results for the data in the realistic model show reflections are removed ideally as well (Fig. 4b). One can see that the result of diffraction separation is relatively close to the ideal one (Fig. 4a) in terms of diffracted/scattered waves produced by the bottom fractured layer (Fig. 4b). There is a perfect correspondence of kinematic properties of diffracted waves and rather good match of dynamic behavior between the ideal waves and diffraction separation results. One can observe that, in this case, the diffractions produced by the top fractured layer are recovered as well. Their behavior is like the behavior of the diffractions produced by the bottom layer. Both fracture layers have identical geometric and amplitude properties. Therefore, one should expect similar properties of diffractions from these layers that provide an additional confirmation that the separation algorithm works properly.

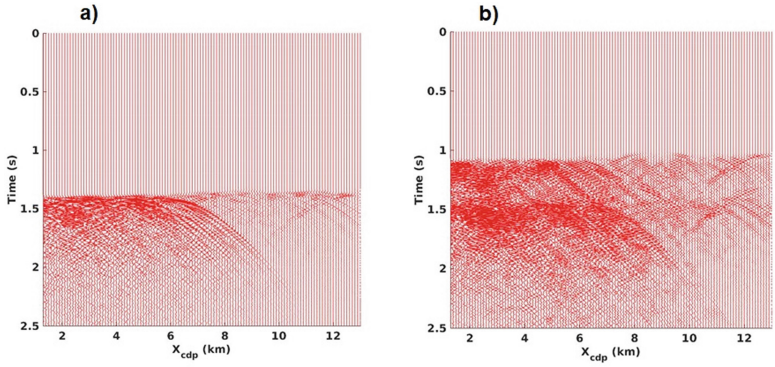

Fig. 4. Realistic data: a) the ideal separation; b) results of the data domain diffraction separation.

3 Diffraction Imaging

For diffraction image construction, the concept of selective images is used [15]:

$$SelectiveImage(\overline{x};\alpha,\beta) = \int T_{qp}^{gbs}(x_s;\overline{x};\alpha,\beta;\omega)\cdot T_{qp}^{gbr}(x_r;\overline{x};\alpha,\beta;\omega) \cdot d(x_r;x_s;\omega)dx_r dx_s d\omega \quad (4)$$

Here $\boldsymbol{d}$ is the seismic data, $\boldsymbol{x_r}/\boldsymbol{x_s}$ is the source/receiver coordinate, $\boldsymbol{\omega}$ is the frequency, $\boldsymbol{\alpha}$, $\boldsymbol{\beta}$ are the dip and opening angles, $\boldsymbol{T_{qp}^{gbs(r)}}$ are the source(receiver) stacking weights. To calculate the stack image corresponding to the standard migration of seismic data, it is necessary to sum the selective images with respect to all available dip and opening angles.

3.1 Diffraction Imaging Resolution

A detailed examination of individual selective images and their partial sums shows that their resolution is different. Using the example of a model and data with diffractors only (Fig. 3a), one can observe that the resolution increases as the number of selective images increases, corresponding to an increase in the range of dip angles (Fig. 5). Thus, the larger the range of dip angles is available for constructing a diffraction image, the better its spatial resolution. Note that, for the construction of diffraction images, the largest range of dip angles will be available if the imaging procedure uses diffracted/scattered waves only. The presented simple example clearly shows this observation (Fig. 5).

3.2 Diffraction Imaging Comparison

Next experiments provide the comparison of the diffraction imaging based on an asymmetric summation of selective images constructed for the seismic data without and with diffracted/scattered wave separation. First, simple data and model is considered. When data contains diffractions and reflections, «full» sum of selective images provides reflections events mainly while diffractions are almost invisible (Fig. 6a). Partial sum of selective image provides diffraction events mainly (Fig. 6a, 6b). These partial images have the same resolution when partial images are constructed for the ideal diffraction data (Fig. 5a, 5b). However, when the diffraction separation algorithm provides the data that contains diffractions only then «full» sum of selective images provides diffractions only as well and the resolution of such image is higher than resolution of the diffraction images that are a partial sum of selective images (Fig. 7a, 7b, 7c). Also «full» sum of selective images provides comparable results for both cases: ideal diffractions identification (Fig. 5a) and application of diffraction separation algorithm (Fig. 7a). The conclusions from these experiments are obvious: a) one needs to separate diffractions in seismic data before diffraction imaging application; b) the proposed diffractions separation algorithm provides rather good diffraction identification so that their image is close to the image of ideal diffractions.

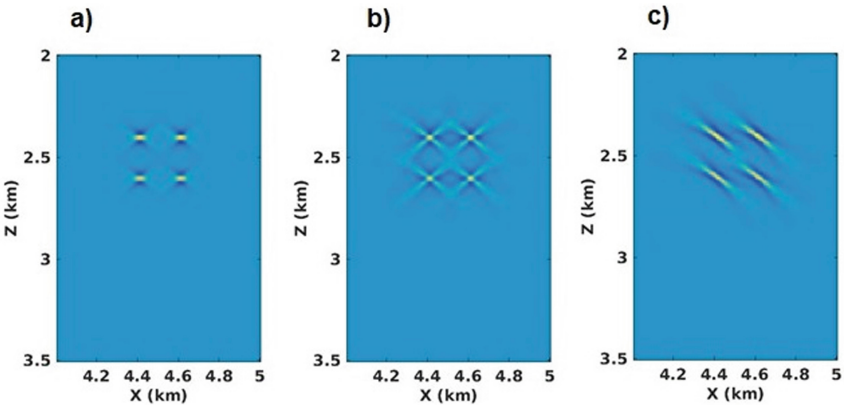

Fig. 5. Image resolution, i.e. image of the simple data with the diffractions only: a) «full» sum of selective images: a $= [-40° : 1° : 40°]$; b) partial sum of selective images, a $= [-40° : 1° : -25°]$ and a $= [25° : 1° : 40°]$; c) partial sum of selective images, a $= [-40° : 1° : -25°]$.

Then image results are provided for realistic synthetic model and data. Three datasets are used for diffraction imaging: the original seismic data containing all wave types, the data after ideal subtraction, where only the waves diffracted/scattered by the bottom fracture layer remain, and the data after diffraction separation. First, for the initial seismic data, a «full» image (Fig. 8b) and a diffraction image (Fig. 8c) were constructed, where selective images for the angles a $= [-40° : 1° : 40°]$ in the first case, and for the second a $= [-40° : 1° : -25°]$ and a $= [25° : 1° : 40°]$. The diffraction image shows two layers with fractures and faults, but the remnants of reflected waves are also

visible. Then, to the ideal diffraction data and the data after diffraction separation, a similar imaging procedure was applied for the angles a $= [-40^\circ : 1^\circ : 40^\circ]$. One can see a significant difference in diffraction images got from the data without preliminary separation (Fig. 8c) and from ideal data containing only scattered waves (Fig. 8d). The image is much more focused and less noisy in the second case. The last is the best achievable result in the bottom fracture layer image.

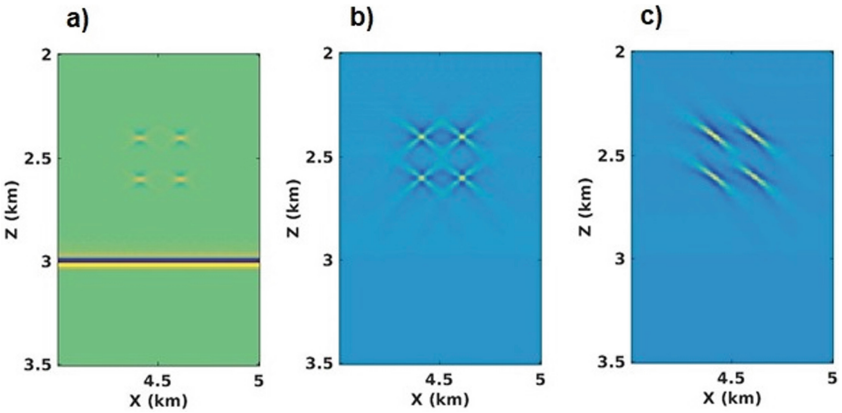

Fig. 6. Image of the simple data with the reflections and diffractions: a) «full» sum of selective images: a $= [-40^\circ : 1^\circ : 40^\circ]$; b) partial sum of selective images, a $= [-40^\circ : 1^\circ : -25^\circ]$ and a $= [25^\circ : 1^\circ : 40^\circ]$; c) partial sum of selective images, a $= [-40^\circ : 1^\circ : -25^\circ]$.

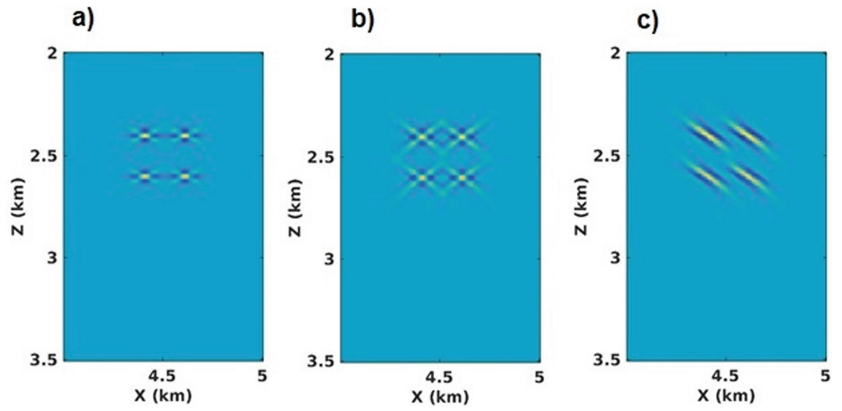

Fig. 7. Image of the simple data after diffraction separation: a) «full» sum of selective images: a $= [-40^\circ : 1^\circ : 40^\circ]$; b) partial sum of selective images, a $= [-40^\circ : 1^\circ : -25^\circ]$ and a $= [25^\circ : 1^\circ : 40^\circ]$; c) partial sum of selective images, a $= [-40^\circ : 1^\circ : -25^\circ]$.

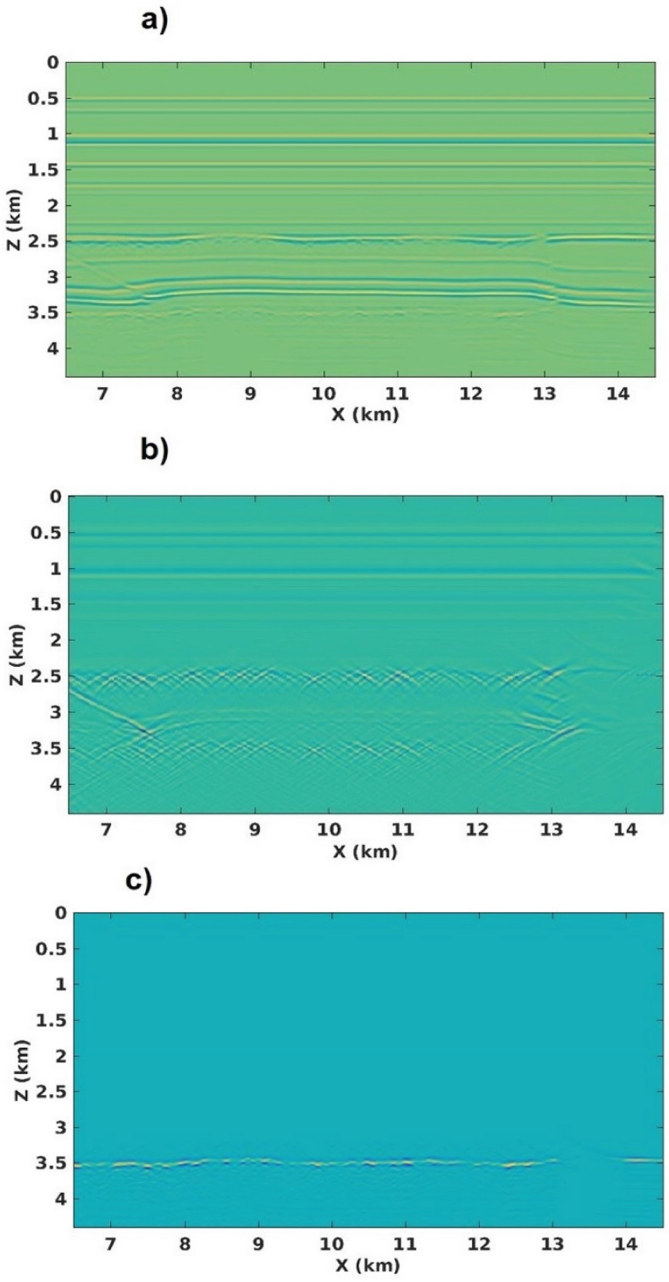

Fig. 8. a) Realistic model containing two fractures layers; b) «full» sum of selective images of the data without any processing: a $= [-40^\circ : 1^\circ : 40^\circ]$; c) partial sum of selective images of the data without any processing, a $= [-40^\circ : 1^\circ : -25^\circ]$ and a $= [25^\circ : 1^\circ : 40^\circ]$; d) «full» sum of selective images of the data with the «ideal» diffractions: a $= [-40^\circ : 1^\circ : 40^\circ]$.

More detailed consideration of the images near the bottom layer fractured zone illustrates the advantages of the diffraction separation in the data before diffraction imaging (Fig. 9). The image result of data after diffraction separation (Fig. 9d) is close to the ideal result (Fig. 9c). It is more focused, less noisy, and more consistent with the model (Fig. 9a) than the selective diffraction image of raw data (Fig. 9b).

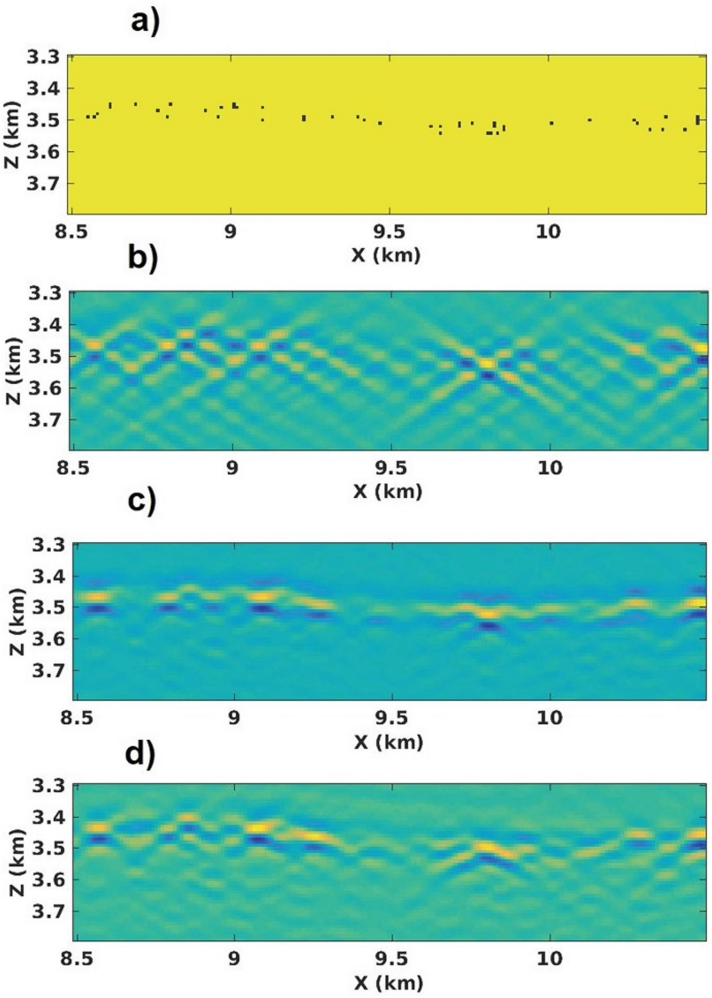

Fig. 9. a) The model area containing bottom layer with fractures. In the same area: b) partial sum of selective images of the data without any processing, a $= [-40° : 1° : -25°]$ и a $= [25° : 1° : 40°]$; c) and d) are «full» sum of selective images of the data with the «ideal» and data after diffraction separation using different kinematic behavior of the reflections and diffractions: a $= [-40° : 1° : 40°]$.

4 Conclusions

The paper presents the new workflow for the seismic data processing of the diffracted/scattered waves. It uses preliminary diffraction separation in the data domain with the following application of diffraction imaging procedure. The new algorithm for the diffraction separation in the data domain is developed and tested. The algorithm uses the different kinematic behavior of reflected and diffracted/scattered waves in common offset domain. The reflections removal and diffractions enhancement are two of the major steps in the procedure. The diffraction imaging procedure uses Gaussian beam for the construction of selective images. The paper provides an investigation of the influence of the diffraction separation in the data do-main on the diffraction imaging procedure. On the simple and realistic datasets, the investigation shows that a preliminary wave separation in the data domain provides a relatively good approximation of diffracted/scattered waves. Further construction of diffraction images of the diffracted/scattered component only makes it possible to get a more focused and less noisy image than when constructing selective diffraction images of the full wave-field.

Acknowledgments. The work is supported by RSF grant 21-71-20002. The work's numerical results were obtained using the computational resources of Peter the Great Saint-Petersburg Polytechnic University Supercomputing Center (scc.spbstu.ru).

References

1. Liu, E., et al.: Fracture characterization by integrating seismic-derived attributes including anisotropy and diffraction imaging with borehole fracture data in an offshore carbonate field. In: International Petroleum Technology Conference, IPTC-18533 (2015)
2. De Ribet, B., Yelin, G., Serfaty, Y., Chase, D., Kelvin, R., Koren, Z.: High resolution diffraction imaging for reliable interpretation of fracture systems. First Break **35**, 43–47 (2017)
3. Shtivelman, V., Keydar, S.: Imaging shallow subsurface inhomogeneities by 3D multipath diffraction summation. First Break **23**, 39–42 (2005)
4. Kanasewich, E.R., Phadke, S.M.: Imaging discontinuities on Seismic Sections. Geophysics **53**, 334–345 (1998)
5. Fomel, S., Landa, E., Taner, T.: Poststack velocity analysis by separation and imaging of seismic diffractions. Geophysics **72**, 89–94 (2007)
6. Moser, T.J., Howard, C.B.: Diffraction imaging in depth. Geophys. Prospect. **56**, 627–642 (2008)
7. Landa, E., Fomel, S., Reshef, M.: Separation, imaging, and velocity analysis of seismic diffractions using migrated dip-angle gathers. In: 72nd SEG Annual Meeting Expanded Abstracts, pp. 2176–2100 (2008)
8. Reshef, M., Landa, E.: Poststack velocity analysis in the dip-angle domain using diffractions. Geophys. Prospect. **57**, 811–821 (2009)
9. Klokov, A., Baina, R., Landa, E.: Separation and imaging of seismic diffractions in dip angle domain. 72nd EAGE Annual Meeting Expanded Abstracts (2010)
10. Klokov, A., Fomel, S.: Separation and imaging of seismic diffractions using migrated dip-angle gathers. Geophysics **77**, S131–S143 (2012)
11. Decker, L., Merzlikin, D., Fomel, S.: Diffraction imaging and time-migration velocity analysis using oriented velocity continuation. Geophysics **82**, U25–U35 (2017)

12. Zhang, D., Fei, T., Tsingas, C., Luo, Y.: Efficient wave equation based diffraction imaging. Geophysics **84**, S389–S399 (2019)
13. Wang, H., Liu, X., Chen, Y.: Separation and imaging of seismic diffractions using a localized rank-reduction method with adaptively selected ranks. Geophysics **85**, V497–V506 (2020)
14. Bansal, R., Imhof, M.: Diffraction enhancement in prestack seismic data. Geophysics **70**, 73–79 (2005)
15. Protasov, M.I., Reshetova, G.V., Tcheverda, V.A.: Fracture detection by Gaussian beam imaging of seismic data and image spectrum analysis. Geophys. Prospect. **64**, 68–82 (2016)
16. Bakulin, A., et al.: Nonlinear beamforming for enhancement of 3D prestack land seismic data. Geophysics **85**, V283–V296 (2020)
17. Berkovitch, A., Belfer, I., Hassin, Y., Landa, E.: Diffraction imaging by multifocusing. Geophysics **74**, WCA75–WCA81 (2009)